ACS Catalysis

pubs.acs.org/acscatalysis
Research Article

Predicting the Stability of Single-Atom Catalysts in Electrochemical Reactions

Giovanni Di Liberto, Livia Giordano,* and Gianfranco Pacchioni*

Cite This: ACS Catal. 2024, 14, 45−55
Read Online

ACCESS | Metrics & More | Article Recommendations | Supporting Information

ABSTRACT: The attention toward single-atom catalysts (SACs) for electrochemical processes is growing at an impressive pace. Electronic structure calculations play an important role in this race by providing proposals of potentially relevant catalysts based on screening studies or on the identification of descriptors of the chemical activity. So far, almost all of these predictions ignore a crucial aspect in the design of a catalyst: its stability. We propose a simple yet general first-principles approach to predict the stability of SACs under working conditions of pH and applied voltage. This is based on the construction of a thermodynamic cycle, where part of the information is taken from experiment and the rest from density functional theory (DFT) calculations. In particular, we make use of the formalism of Pourbaix diagrams to investigate the stability of SACs in reductive or oxidative conditions and we identify those that show a pronounced tendency to dissolve or to form other chemical species. Applying the procedure to four transition metal atoms, Cr, Mn, Fe, and Co, and to three supports, N-doped graphene, carbon nitride, and covalent organic frameworks, we show that a key factor in determining the final stability is the binding energy of the free metal atom to the support. The results show that several potentially very good catalysts in key electrochemical reactions are, in fact, dramatically prone to dissolution or transformation in other chemical species, suggesting that every prediction of the SAC's catalytic activity should be accompanied by a parallel investigation of the stability.

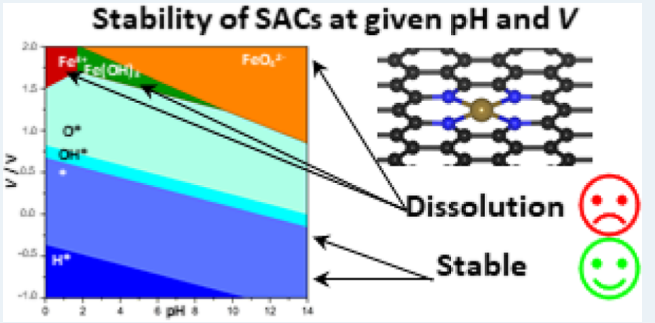

KEYWORDS: *single-atom catalyst, DFT, Pourbaix diagram, stability, electrochemical reactions*

INTRODUCTION

Catalysis with single metal atoms is a potentially relevant new frontier with an expected impact on the incoming energy and environmental transition.[1−4] A single-atom catalyst (SAC) is made by a transition metal (TM) atom embedded in a solid matrix.[5−9] SACs bridge the two worlds of homogeneous and heterogeneous catalysts.[10−14] The former are often more active but the latter are more stable and for this reason are involved in the vast majority of technological applications of catalysis.[15] Indeed, an SAC is a heterogeneous catalyst with atomic dispersion and a well-defined local environment. It offers the possibility of maximizing the active phase, reducing the metal loading, and playing with the local environment to tune the catalytic activity.[14,16−18] Both aspects are of paramount importance in the design of new efficient materials to address future challenges in terms of critical raw materials and sustainability.

Virtually every solid surface has been used to support SACs: oxides, sulfides, metals, carbon-based materials, etc.[19−25] The latter gained increasing attention in the last years and are widely used in electrochemical reactions of interest, such as the hydrogen evolution (HER), the oxygen evolution (OER), the oxygen reduction (ORR) reactions, nitrogen fixation, or CO_2 electroreduction.[26−32] Rationalizing the behavior of SACs is challenging due to their atomistic nature, which renders their experimental characterization difficult. Computational studies offer a powerful tool to increase our understanding of their chemistry and possibly predict new promising candidates. The number of high-throughput and artificial intelligence-driven screening works in this area is steadily growing.[27,33−45]

However, so far, the attention of the computational community has been largely focused on the activity and, to some extent, on the selectivity of new SACs, with much less attention to their stability. In thermal catalysis, the focus is on the tendency of SACs to diffuse and aggregate to form metal nanoparticles (sintering).[46,47] For instance, Su et al. studied the partial pressure conditions of CO and the temperature range within which individual Pt atoms are more stable than Pt nanoparticles on CeO_2, finding that when Pt atoms are

Received: October 9, 2023
Revised: November 17, 2023
Accepted: November 28, 2023
Published: December 9, 2023

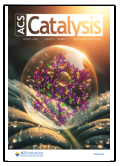

incorporated into the CeO_2 lattice, this results in greater stability than for Pt atoms adsorbed on CeO_2 terraces and steps.[48] Experimentally, the preparation of thermally stable SACs remains a challenging task.[49]

Things are even more complicated in electrochemical reactions where solvent, pH, and applied voltage can result in a variety of behaviors of the metal species, including demetalation. Dobrota et al. investigated by means of DFT the nature of various TM atoms in a graphene monovacancy finding that the metal centers are covered with H, O, or OH groups at any potential or pH in the water thermodynamic stability region.[50] A similar conclusion was reached by the same group for TM atoms stabilized in N-doped graphene.[51] Besides formation of stable complexes at the TM centers, demetalation is a serious problem in electrochemical reactions, but relatively few theoretical studies have been dedicated to this problem. Holby et al. performed DFT calculations to identify the conditions of stability of Fe atoms embedded in N-doped bilayer graphene as a function of pH and potential in ORR using the bulk metal as a reference for the stability analysis.[52] Cho et al. compared the stability of SACs made by the same metal, Pt.[53]

It goes without saying that stability is a crucial aspect of every catalyst, and SACs are no exception. SACs are not static objects and can evolve during the reaction.[54] In electrocatalysis, besides diffusion and aggregation, the metal atom can change the oxidation state, react with the environment, in particular the solvent, and form new chemical species including stable complexes that lead to leakage of the metal atoms and dispersion in the solvent (dissolution).[55] This is particularly relevant for oxidative processes. Of course, one cannot exclude that, as in thermal catalysis, aggregation of metal atoms occurs in electrocatalytic experiments also, especially under reductive conditions. To take this possibility into account, one should extend the analysis including metal aggregation and metal diffusion as additional steps. This is particularly challenging, as the driving force for the initial steps of metal nucleation and growth depends on the particle size and shape. All of these effects lead to the deactivation of the catalyst.

We propose a simple but effective approach to estimate the relative stability of an SAC at given electrochemical conditions of pH and applied voltage. This is based on the well-known formalism of Pourbaix diagrams[52,56−59] and on the construction of a thermodynamic cycle from which the redox potential of a SAC can be derived. The novelty of the work is that in the thermodynamic cycle, we introduce two steps, one referred to the desorption of the TM from the solid matrix in the gas phase and the second to the aggregation of gas-phase TM atoms to form the bulk solid (cohesive energy). In this way, we can identify the binding energy of the TM atom to the support as a very robust descriptor of the stability of a SAC in electrocatalytic reactions.

By studying four examples of TM atoms (Cr, Mn, Fe, and Co) stabilized on carbon-based supports (nitrogen-doped graphene, 4N-Gr, carbon nitride, C_3N_4, and covalent organic frameworks, COFs), we will show that most of the SACs considered are unstable in operative conditions, with relevant consequences for some supports such as carbon nitride, where none of the atoms studied are stable (at least in the considered coordination environment). Using this approach, one can easily get a first estimate of the stability of a SAC. This estimate can then be easily refined or improved, if necessary, by increasing the level of accuracy of the DFT-derived quantities that enter the determination of the thermodynamic stability. The results suggest that a preliminary analysis of the stability should be included in every study aiming at screening novel SACs.

COMPUTATIONAL DETAILS

DFT calculations including spin polarization were performed by the VASP[60−62] package using the generalized gradient approximation, as implemented in the Perdew−Burke−Ernzerhof (PBE) functional.[63] Dispersion forces have been included according to Grimme's D3 parametrization.[64] The valence electrons were expanded on a set of plane waves with a kinetic energy cutoff of 400 eV, whereas the core electrons were treated with the projector augmented wave (PAW) approach.[65,66] The threshold criteria for electronic and ionic cycles were set to 10^{-5} eV and 10^{-3} eV/Å, respectively. The sampling of the reciprocal space was adopted according to the dimension of the simulated cells to provide converged results. A 5 × 5 × 1 Monkhorst−Pack k-point grid[67] was used to sample the reciprocal space for graphene and N-doped graphene and reduced to 1 × 2 × 1 for C_3N_4 because of the cell dimensions. We fully optimized a graphene nanosheet (a = b = 2.468 Å, γ = 120°) with a working vacuum layer of 15 Å to avoid spurious effects due to the interaction with a periodic replica of the system along the nonperiodic direction. A 4 × 4 × 1 supercell was considered for graphene-based systems (a = b = 9.870 Å, γ = 120°).[68−70] The nitrogen-doped graphene model was generated by creating a C divacancy, replacing four C with N atoms, and relaxing the atomic coordinates. The metal atoms were embedded in the cavity. We then considered a corrugated C_3N_4 layer characterized by heptazine pores and we optimized the lattice parameters (a = 13.846 Å, b = 6.923 Å, γ = 120°).[71,72] Finally, we took a recently established 2D COF having a cavity able to host a metal atom coordinated by four nitrogen atoms. This structure was obtained by a combination of metallophthalocyanine and pyrazine and was studied for CO_2 and N_2 reduction.[73,74] The optimized lattice parameters are a = 20.318 Å, b = 20.318 Å, γ = 90°.[75] Metal atoms were adsorbed inside the pore. In all cases, we checked for the possible formation of several minima.[70] The reported structures correspond to global minima. Representative structures are reported in Figure S1.

The calculated binding energies, E_b, computed with respect to the free TM atoms and the support, are reported in Table S1, where we can appreciate that, on average, the COF binds metal atoms more strongly than 4N-Gr that in turn is more active in stabilizing metal atoms than C_3N_4.

We considered the possible formation of adsorbates typical of the reduction and oxidation reactions of water splitting. Notice that for simplicity, we restricted the analysis to the formation of H*, OH*, O*, and OOH* intermediates, which are known to form on metal electrodes and that are assumed to form also on SACs

$$*+H^+ + e^- \rightarrow H^* \quad (1)$$

$$H_2O + * \rightarrow OH^* + H^+ + e^- \quad (2)$$

$$H_2O + * \rightarrow O^* + 2H^+ + 2e^- \quad (3)$$

$$2H_2O + * \rightarrow OOH^* + 3H^+ + 3e^- \quad (4)$$

In reality, recent studies have shown that on SACs, other intermediates can form,[70,76,77] thus resulting in more complex

https://doi.org/10.1021/acscatal.3c04801
ACS Catal. 2024, 14, 45−55

phase diagrams. However, for the purpose of this work, i.e., illustrating the procedure, these new intermediates have been neglected, although their formation should be taken into account for quantitative studies.

The reaction energies (ΔE) of each intermediate were calculated with respect to water and the free catalyst as references. The Gibbs energies were evaluated by adding the zero-point energy correction and entropy terms. The first were calculated in a harmonic fashion (details can be found in Section S1 and in ref 77). Entropies of gases were taken from the international tables, and the entropy of solid-state species was considered equal to zero,[77] see Section S1.[78] Given the specific purpose of this study, which is to compare the stability of TM atoms embedded in different frameworks, the adopted approximation can be considered acceptable. The calculated Gibbs free energies of H*, OH*, O*, and OOH* are reported in Tables S4−S6. The potential dependence was included within the framework of the computational hydrogen electrode (CHE).[79]

RESULTS AND DISCUSSION

Pourbaix Diagrams Including Dissolution of the SAC.

To evaluate the tendency of a chemical species to transform into another, one has to consider the Gibbs free energy associated with the reaction. This can be done by constructing a simple thermodynamic cycle (see Figure 1, referred to as Fe

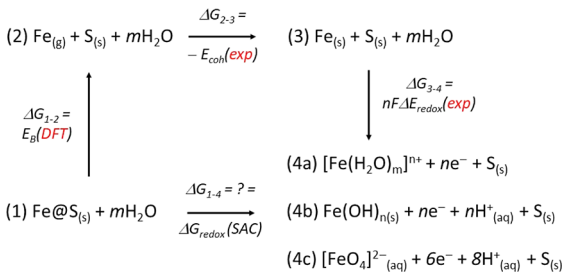

Figure 1. Thermodynamic cycle to determine the Gibbs free energy of the dissolution process (redox process) of a SAC. We refer as an example to the dissolution of Fe@S (S = C_3N_4, 4N-Gr, and COF) in aqueous solution.

SAC). The target reaction is described by ΔG_{1-4} and can lead to different products: the metal atom can dissolve and form aquo-complexes, see 4(a) in Figure 1, or for specific conditions of pH and voltage, new oxide or hydroxide species can form and either precipitate or remain in solution, see 4(b) and 4(c) in Figure 1. During these processes, the metal atom can vary the oxidation state giving rise to a considerable number of products. Section S2 reports all the dissolution processes considered in this work for the four atoms of interest, Cr, Mn, Fe, and Co. ΔG_{1-4} is the unknown target quantity which can be obtained by breaking up the process in intermediate steps whose associated Gibbs free energies are either accessible experimentally or can be obtained from DFT calculations.

This is the case of the first step of the thermodynamic cycle, the separation of the metal atom from the binding matrix; see Figure 1. ΔG_{1-2} corresponds to the binding energy of a gas-phase TM atom to the site where this is stabilized in the SAC structure. ΔG_{1-2} is not accessible experimentally but can be computed theoretically at the desired level of accuracy. This quantity is also the only variable of the entire cycle that needs to be computed, and as we will show below, it provides a robust descriptor of the overall stability of the SAC. The next step, ΔG_{2-3}, corresponds to the inverse of the sublimation of a bulk metal, as the gas-phase TM atoms condense into a bulk lattice. This is the inverse of the metal cohesive energy, a quantity that can be accessed both experimentally and computationally. Here we decided to use the measured values of the cohesive energies of the four metals of interest, Cr, Mn, Fe, and Co.[80,81] The last step, which closes the cycle, corresponds to a classical redox process where a bulk metal is oxidized to one of the possible species that can form (aquo-complexes, oxides, hydroxides, etc.). The corresponding ΔG_{3-4} is also tabulated as it corresponds to the redox potential for the reaction. Notice that while Pourbaix diagrams have been reported previously, these are typically referred to as the bulk metal; here we introduce the notion of stability with respect to the isolated atom and its interaction with the support. The inclusion of the desorption of the TM atom in the gas phase in the cycle allows us to disentangle the binding energy of the TM to the support from the contribution of the metal−metal bond in the bulk and to identify a useful descriptor of the process, easily accessible via DFT (all of the remaining quantities can be taken from experiment). Of course, one could directly correlate process (1) to (3) in Figure 1, resulting in a rigid shift of the value of the descriptor but losing the information about the strength of the bond of the TM atom to the support as a proxy of the stability of the SAC.

The thermodynamic cycle reported in Figure 1 allows us to determine the stability of the SAC against dissolution by using the binding energy of the TM atom to the support. This is the only computed quantity. We considered the possibility of having the SAC in its clean state or being covered by specific adsorbates (intermediates). The free energy of the adsorbates as a function of pH and voltage was calculated by using the CHE,[79] as reported in Section S3, according to the following equation

$$\Delta G_x = \Delta G_x^{\circ} - nV_{\mathrm{SHE}} - nk_{\mathrm{b}}T\ln(10)\mathrm{pH} \quad (5)$$

where n is the number of exchanged electrons. The stability diagram was constructed by taking the most stable species for each value of the (pH, V) pair. As an example of the overall approach, we discuss in detail the Pourbaix diagram of Fe@4N-Gr, see Figure 2. Under HER conditions ($V \sim 0$ V at pH = 0), the catalyst is expected to be stable in its clean state (no adsorbed species), indicated with *, the free adsorption site, while under a reducing applied potential, it becomes covered by H atoms, H*. Working at the equilibrium potential for the O_2/H_2O redox ($V \sim 1.23$ V at pH = 0), the Fe atoms are bound to O atoms forming O* species at low pH, while the Fe atoms are expected to dissolve in conditions of basic pH. At the higher potentials typical of OER ($V \sim 1.5$ V), the catalyst becomes unstable against dissolution at any pH. At very low pH, <2, the catalyst will dissolve leading to Fe^{3+} aquo complexes while higher pH values promote the precipitation of solid $Fe(OH)_3$. At very high potentials and pH, the dissolution to FeO_4^{2-} becomes favorable, see Figure 2.

Of course, the nature of the metal center is essential in determining the stability of a SAC. Figure 2 compares the Pourbaix diagrams for Cr, Mn, and Co atoms supported on 4N-Gr with that of Fe, just discussed. Cr@4N-Gr tends to dissolve in rather strong oxidative conditions, $V > 1$ V. At acid pH values, it forms Cr^{3+} aquo complexes but at higher pH, $Cr(OH)_3$ is favored. Co@4N-Gr is stable in its clean state in both reducing and oxidative conditions, while Mn@4N-Gr and

https://doi.org/10.1021/acscatal.3c04801
ACS Catal. 2024, 14, 45−55

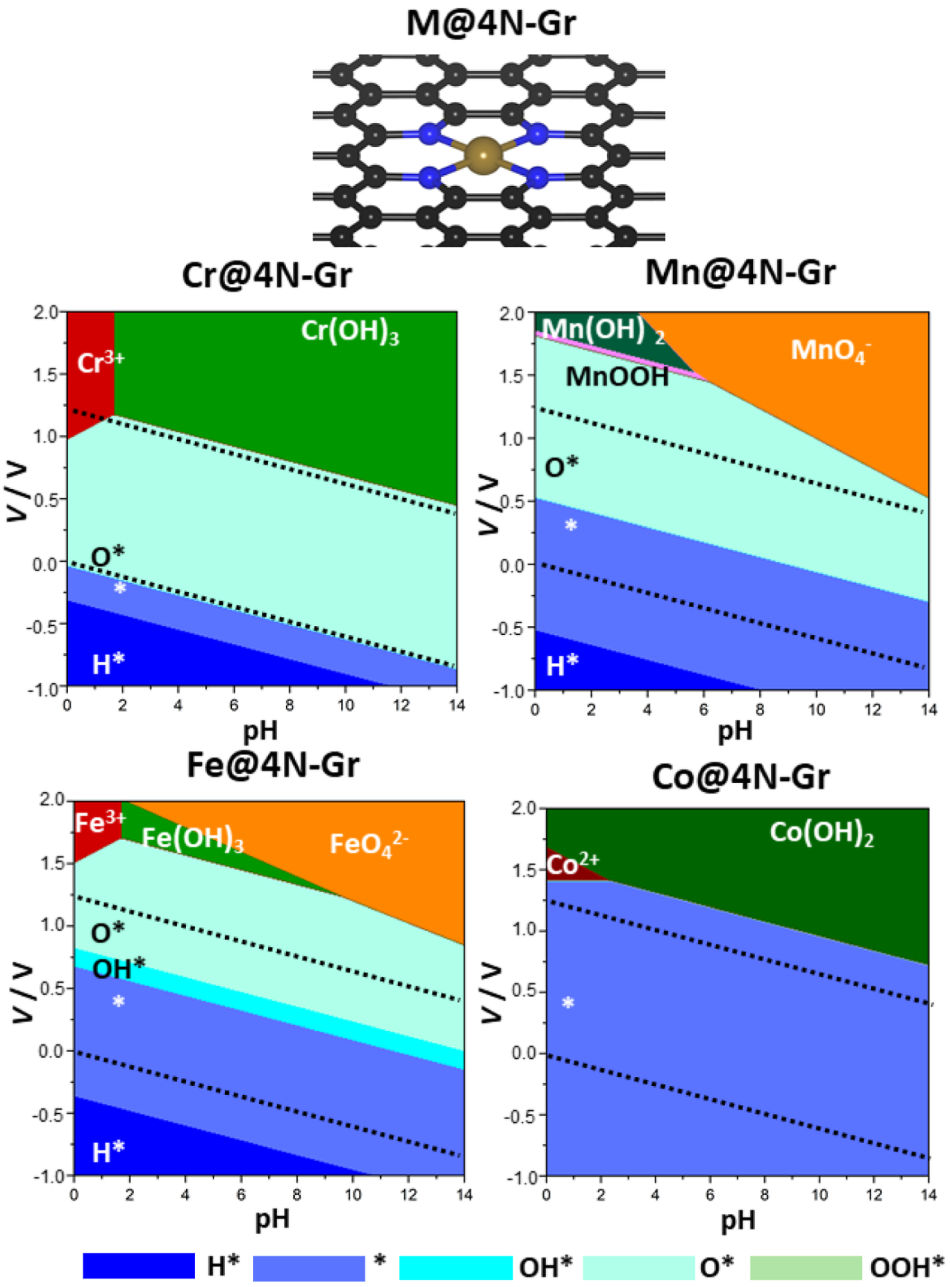

Figure 2. Pourbaix diagrams of Cr@4N-Gr, Mn@4N-Gr, Fe@4N-Gr, and Co@4N-Gr. The pH−voltage window where the catalyst is stable in the SAC state either clean or covered by some intermediate is reported with colors identifying H*, *, OH*, O*, and OOH* states. Black dashed lines indicate the redox levels of H^+/H_2 and O_2/H_2O couples.

Fe@4N-Gr tend to be covered by adsorbed species. All SACs tend to dissolve or precipitate at high oxidative potentials depending on the working conditions.

The supporting matrix affects the stability even more dramatically than changing the TM atom. Figure 3 shows the Pourbaix diagrams of Cr, Mn, Fe, and Co bound to the heptazine site of a carbon nitride nanosheet (C_3N_4), see Figure 3. In this site, the metal atom can be easily accommodated but with relatively loose bonds with the carbon matrix. This has dramatic effects on the overall stability, as the four SACs are no longer stable, neither under reducing nor oxidizing conditions. More specifically, Mn@C_3N_4 dissolves to Mn^{2+} solvated ions at low pH and reducing conditions, while it forms $Mn(OH)_2$ as the pH increases. In oxidizing conditions, Mn assumes higher oxidation states. Fe@C_3N_4 is expected to be stable only for applied potentials below −0.5 V in acid conditions. At the same potential but higher pH values, Fe@C_3N_4 is expected to lead to the precipitation of $Fe(OH)_2$. Similarly, Co@C_3N_4 is stable only in strong reducing conditions since it tends to form Co^{2+} ions in solution or $Co(OH)_2$ at moderate applied voltages. In short, SACs supported on the heptazine pore of a C_3N_4 nanosheet are expected to be labile, as shown in Figure 3. The fact that in all cases, the stability of TM anchored on the heptazine pore of C_3N_4 is very low suggests that in real systems, the structure of the active site is probably different from the typically assumed (heptazine) one but has not been identified yet.

An opposite case is that of SACs stabilized in COFs, Figure 4, since these materials strongly anchor the TM atoms.[82,83] The overall stability of the TM@COF is significantly

https://doi.org/10.1021/acscatal.3c04801
ACS Catal. 2024, 14, 45−55

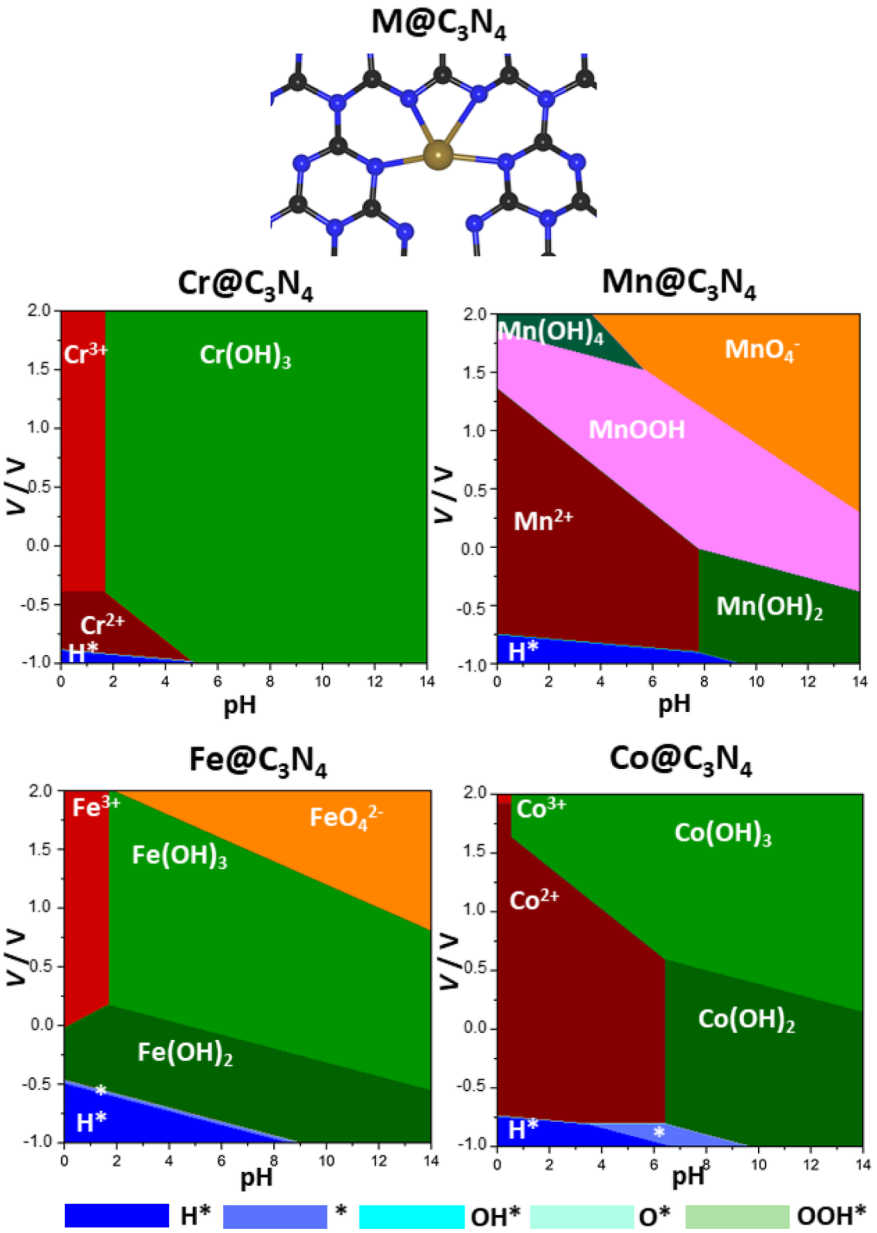

Figure 3. Pourbaix diagrams of $Cr@C_3N_4$, $Mn@C_3N_4$, $Fe@C_3N_4$, and $Co@C_3N_4$. The pH−voltage window where the catalyst is stable in the SAC state either clean or covered by some intermediate is reported with colors identifying H*, *, OH*, O*, and OOH* states. Black dashed lines indicate the redox levels of H^+/H_2 and O_2/H_2O couples.

improved. The Mn@COF and Fe@COF are very stable, and their dissolution is expected only at strongly oxidative and high pH conditions; Cr@COF and Co@COF are so stable that they are not expected to dissolve in the entire range of pH and voltage investigated.

The discussion above shows that different supports can stabilize the same metal atom to a very different extent. Some supports give rise to extremely stable compounds, while others are prone to leakage of the metal atoms via dissolution or formation of more stable species. The importance of determining the relative stability of the SAC could be related in principle to the activity of the complex, as one could expect a kind of anticorrelation between stability and activity. To check this effect, we analyzed the case of HER and OER on the 12 systems investigated here (Figure S2) reporting the calculated Gibbs free energies of HER and OER intermediates against the binding energy of the SACs. While some general trend can be observed, e.g., the Gibbs free energy of H* on C_3N_4-based SACs (lower stability) is on average closer to zero (higher activity) than the one of 4N-Gr and COF, there are notable exceptions (e.g., Co@4N-Gr and Co@COF). Even more complex is the case of OER, so that no clear anticorrelation between stability and activity can be established, at least at this level.

It must be mentioned that the assessment of the reactivity of SACs is often more complex than usually assumed, due to their peculiar reactivity that may deviate from that of extended surfaces. The main consequences are the breaking of scaling relations and the formation of unconventional intermediates not present on metal electrodes.[76,77] Different reactivity descriptors are available nowadays for extended catalysts, such as the electrochemical-step symmetry index[84] and the free

https://doi.org/10.1021/acscatal.3c04801
ACS Catal. 2024, 14, 45−55

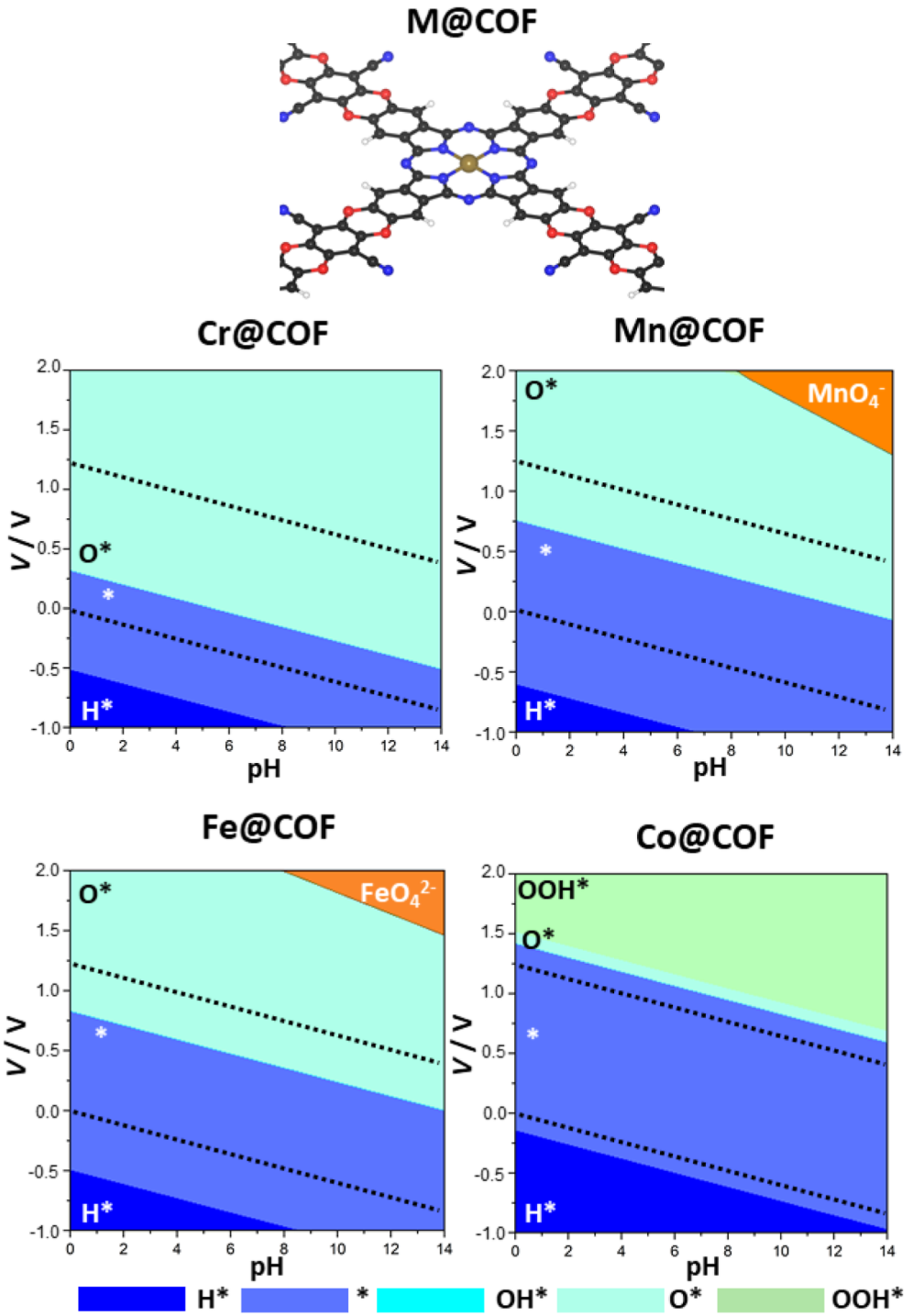

Figure 4. Pourbaix diagrams of Cr@COF, Mn@COF, Fe@COF, and Co@COF. The pH−voltage window where the catalyst is stable in the SAC state either clean or covered by some intermediate is reported with colors identifying H*, *, OH*, O*, and OOH* states. Black dashed lines indicate the redox levels of H^+/H_2 and O_2/H_2O couples.

energy span model $[G_{max}(\eta)]$.[85] However, the application of these tools to the assessment of the reactivity of stable SACs requires dedicated investigations.

Rational Design of Stable SACs. The stability of SACs is a function of both the TM and the support, although the support plays a much more important role. Here we show that the binding energy, E_b, of an isolated metal atom to the support is a simple but reliable descriptor of the stability of a SAC.[86] In fact, based on the thermodynamic cycle reported in Figure 1, it is possible to calculate the minimum value of E_b required to guarantee that a SAC is stable under given conditions. More specifically, if we set the external conditions of pH and voltage, it is possible to evaluate a threshold value ε_b that makes a specific SAC stable toward dissolution (see Section S2 for the processes considered in this work).

Figure 5a (Table S9) shows the minimum values of the binding energy required to have a clean SAC that should not dissolve at $V = 0$ V and pH = 0, i.e., close to the equilibrium potential of the H_2O/H_2 redox couple. Similarly, Figure 5b shows the same plot but assumes that it works close to the

https://doi.org/10.1021/acscatal.3c04801
ACS Catal. 2024, 14, 45−55

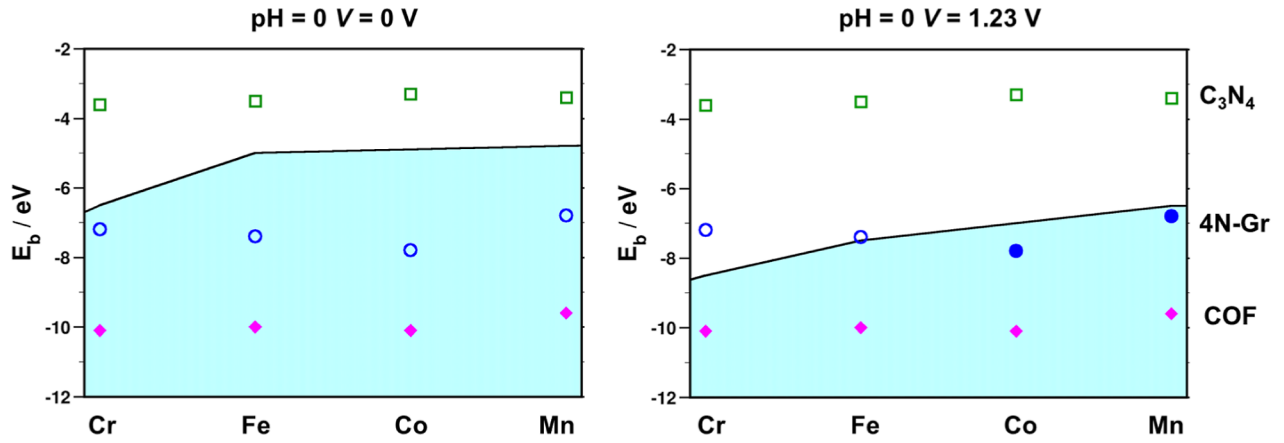

Figure 5. Shaded area corresponds to the region where SACs are expected to show thermodynamic stability at pH = 0 and V = 0.00 V (panel a) and pH = 0 and V = 1.23 V (panel b).

equilibrium potential of the O_2/H_2O redox couple (V = 1.23 V). Of course, analogous values can be computed for different external conditions. The systems identified by a solid symbol correspond to stable species and those indicated by an empty symbol are unstable toward dissolution. The line dividing the stability from the instability region corresponds to the minimum values of E_b(TM) needed to have a stable compound. Figure 5a shows that all of the SACs based on the 4N-Gr and COF are predicted to be stable against dissolution at pH = 0 and V = 0 V. Conversely, C_3N_4-based SACs will tend to dissolve since the binding energy is significantly less negative than the threshold. This reflects the behavior observed in Figures 2−4. Moving to Figure 5b, in this case, C_3N_4 leads to binding energies much weaker than the threshold, resulting in dissolution. On the opposite site are COFs, as they bind TMs very strongly so that they emerge as excellent templates for SACs from the point of view of stability (less reactivity, see above).[82,83] 4N-Gr is the most interesting case since the calculated E_b is close to the threshold value so that Cr@4N−Gr is definitely unstable, Mn@4N-Gr is clearly stable, while Fe@4N-Gr and Co@4N-Gr are borderline. It must be considered that ε_b is a criterion applied to the clean catalyst without adsorbed species. In principle, the resistance against dissolution could be higher by considering the possible formation of adsorbates. Indeed, if the catalyst has borderline behavior, the inclusion of adsorbates should be considered to obtain a more detailed picture. For instance, according to Figure 5b, Fe@4N-Gr could be prone to dissolution, while according to Figure 2, it is stable in a wide range of pH and voltage. This is because a stable O* complex forms on Fe@4N-Gr that makes it resistant to dissolution and is not considered in the analysis of Figure 5b. This example shows the utility of ε_b for a preliminary screening that, however, needs to be refined including the effect of adsorbates when the clean catalyst is near the line separating stability from instability regions.

These simple examples show that the proposed approach can be used to efficiently screen the thermodynamic stability of a SAC. Of course, the reliability of the prediction critically depends on the accuracy of the quantities entering the thermodynamic cycle of Figure 1. Here we decided to use the existing experimental data (redox potential of TMs and cohesive energies of bulk solids) where possible and to resort to DFT for the rest. Needless to say, the level of accuracy of the DFT calculations and of the models used can be systematically improved; the final choice is only a matter of the computer time available. In the following, we show the importance of improving both the method and the model in predicting the stability of SACs by comparing the results discussed so far with those obtained from hybrid functional DFT calculations (method) and from the inclusion of solvent effects (model).

Toward Experimental Complexity. Although the PBE functional adopted so far is sufficiently reliable to obtain general trends, systematic improvements can be obtained by adopting higher levels of functionals such as the hybrid functionals.[87,88] In a similar way, while some general tendencies can be obtained by using models of SACs without including the solvent, it is clear that this plays a direct role in electrochemical reactions. Even the model can be improved and including solvation is the first step to obtain more quantitative predictions.[89−91] Of course, both method and model can be further improved at any desired level, but here we restrict these two aspects to show their impact on the prediction of the thermodynamic stability of SACs under working conditions.

We selected three representative SACs, Fe@C_3N_4, Fe@4N-Gr, and Fe@COF, and we constructed the Pourbaix diagrams using the thermodynamic cycle of Figure 1 but using the PBE0 hybrid functional (25% of exact Fock exchange)[92,93] and compared the results with those obtained at the PBE level. Notice that Fe complexes have usually magnetic ground states, which is where hybrid functionals become relevant.[88] Similarly, we accounted for solvation by adopting the microsolvation[94] model and we constructed the Pourbaix diagrams of the three SACs to compare them with the same in vacuum. The choice of the microsolvation approach, based on the explicit inclusion of a limited number (typically three) of water molecules around the species of interest, is a compromise between accuracy and computational cost.[95] Also, in this case, more accurate models of solvation can be considered, with the only limitation of the computer time involved.

Figure S3 shows the effect of the exchange−correlation functional on the stability of SACs. Not surprisingly, the Pourbaix diagrams of Fe@C_3N_4 (low stability) and Fe@COF (high stability) look unchanged when comparing PBE and PBE0; however, for Fe@4N-Gr, there are quantitative effects, especially when looking at the stability of the reaction intermediates. The stability against dissolution seems to be less affected by the functional. This confirms the important

https://doi.org/10.1021/acscatal.3c04801
ACS Catal. 2024, 14, 45−55

role of the adopted functional in predicting stability and reactivity, although PBE can be considered reasonable when looking at qualitative estimates of trends.

Solvation has a more complex effect. This is because besides the classical solvation contribution to the stability of the reaction intermediates, solvent molecules can bind the catalyst acting as a ligand and compete with reaction intermediates,[96] a typical effect in organometallic chemistry. Even in this case, the effect is negligible for Fe@C_3N_4 and Fe@COF for opposite reasons while it is more pronounced for Fe@4N-Gr, Figure S3.

This simple analysis demonstrates that reliable predictions of new SACs should be made at the highest possible level of theory. Screening of a large set of structures done with not sufficiently accurate methods or with oversimplified models can be useful for a preliminary search of potential candidates but should be followed by accurate analyses of both reactivity and stability in order to be really useful to direct the synthetic efforts.

CONCLUSIONS

The tumultuous growth of studies on SACs in the past decade has stimulated a large number of theoretical investigations aimed at predicting the activity of new systems. So far, attention has been focused on the rational design of SACs whose activity can be tuned by small changes in the surrounding environment, support, or TM atom. Very little attention, however, has been given to the stability of the predicted structures, an aspect that can severely limit the usefulness of these predictions for the synthesis of new catalysts.

In this study, we propose a simple yet efficient scheme to screen the thermodynamic stability of SACs in working conditions of pH and applied voltage. This is based on a thermodynamic cycle and on the construction of Pourbaix diagrams where the stability of various compounds is determined as a function of voltage and pH. We identified a simple and easy approach to compute a descriptor of the stability of the SAC, the binding energy of the TM atom to the support, that can be used to predict the conditions under which a SAC is likely to dissolve or to give rise to more stable chemical species.

The importance of this approach is demonstrated by the fact that our results show that most often SACs are not stable under oxidative conditions and that they exhibit a pronounced tendency to dissolve, thus destroying the active site of the catalyst.

Some supports (e.g., C_3N_4) bind the TM atoms in the heptazine cavities so weakly that the SACs considered are unstable in a large window of pH and voltage; on the other extreme, supports that bind the TM very strongly (e.g., COFs) result in SACs that are stable in virtually every condition, at the expense of much lower activity. The case of TM atoms stabilized in 4N-Gr is intermediate, thus more interesting since these materials can be both stable and active. In these cases, a quantitative prediction of the stability may require the use of more accurate approaches, both from the side of the method and the model, opening the possibility of obtaining very accurate and reliable predictions about the stability of SACs in electrochemical reactions.

We hope that this approach can become a standard for the calculation of the thermodynamic stability of SACs when performing computational screening of novel catalysts.

ASSOCIATED CONTENT

Data Availability Statement

The data reported in this article can be found in the literature cited and can be asked about by the authors upon reasonable request.

Supporting Information

The Supporting Information is available free of charge at https://pubs.acs.org/doi/10.1021/acscatal.3c04801.

Additional DFT data, representative structure of SACs, Gibbs free energies of H*, OH*, O*, and OOH* species plotted against the corresponding adhesion energy of the SAC, Pourbaix diagrams computed with hybrid functionals, redox potentials and relative equations, and equations used to calculate dependence on the pH (PDF)

AUTHOR INFORMATION

Corresponding Authors

Livia Giordano − *Department of Materials Science, University of Milano-Bicocca, 20125 Milano, Italy;* orcid.org/0000-0002-6879-9424; Email: livia.giordano@unimib.it

Gianfranco Pacchioni − *Department of Materials Science, University of Milano-Bicocca, 20125 Milano, Italy;* orcid.org/0000-0002-4749-0751; Email: gianfranco.pacchioni@unimib.it

Author

Giovanni Di Liberto − *Department of Materials Science, University of Milano-Bicocca, 20125 Milano, Italy;* orcid.org/0000-0003-4289-2732

Complete contact information is available at: https://pubs.acs.org/10.1021/acscatal.3c04801

Author Contributions

G.D.L. performed the calculations and the analysis and wrote the first draft. All authors contributed to design the study, analyze the results, and prepare the final draft.

Notes

The authors declare no competing financial interest.

ACKNOWLEDGMENTS

We acknowledge the financial support from the CARIPLO Foundation, project "Carbon dioxide conversion into energy-rich molecules with tailored catalysts". Access to the CINECA supercomputing resources was granted via ISCRAB. We also thank the COST Action 18234 supported by COST (European Cooperation in Science and Technology).

REFERENCES

(1) Wang, A.; Li, J.; Zhang, T. Heterogeneous Single-Atom Catalysis. *Nat. Rev. Chem* **2018**, *2* (6), 65−81.

(2) Kaiser, S. K.; Chen, Z.; Faust Akl, D.; Mitchell, S.; Pérez-Ramírez, J. Single-Atom Catalysts across the Periodic Table. *Chem. Rev.* **2020**, *120* (21), 11703−11809.

(3) Bajada, M. A.; Sanjosé-Orduna, J.; Di Liberto, G.; Tosoni, S.; Pacchioni, G.; Noël, T.; Vilé, G. Interfacing Single-Atom Catalysis with Continuous-Flow Organic Electrosynthesis. *Chem. Soc. Rev.* **2022**, *51* (10), 3898−3925.

(4) Hannagan, R. T.; Giannakakis, G.; Flytzani-Stephanopoulos, M.; Sykes, E. C. H. Single-Atom Alloy Catalysis. *Chem. Rev.* **2020**, *120* (21), 12044−12088.

(5) Qiao, B.; Wang, A.; Yang, X.; Allard, L. F.; Jiang, Z.; Cui, Y.; Liu, J.; Li, J.; Zhang, T. Single-Atom Catalysis of CO Oxidation Using Pt1/FeOx. *Nat. Chem.* **2011**, *3* (8), 634−641.
(6) Vilé, G.; Albani, D.; Nachtegaal, M.; Chen, Z.; Dontsova, D.; Antonietti, M.; López, N.; Pérez-Ramírez, J. A Stable Single-Site Palladium Catalyst for Hydrogenations. *Angew. Chem., Int. Ed.* **2015**, *54* (38), 11265−11269.
(7) Hackett, S. F. J.; Brydson, R. M.; Gass, M. H.; Harvey, I.; Newman, A. D.; Wilson, K.; Lee, A. F. High-Activity, Single-Site Mesoporous Pd/Al2O3 Catalysts for Selective Aerobic Oxidation of Allylic Alcohols. *Angew. Chem.* **2007**, *119* (45), 8747−8750.
(8) Tang, Y.; Asokan, C.; Xu, M.; Graham, G. W.; Pan, X.; Christopher, P.; Li, J.; Sautet, P. Rh Single Atoms on TiO2 Dynamically Respond to Reaction Conditions by Adapting Their Site. *Nat. Commun.* **2019**, *10* (1), 4488.
(9) Di Liberto, G.; Pacchioni, G. Modeling Single-Atom Catalysis. *Adv. Mater.* **2023**, *35*, 2307150.
(10) Cui, X.; Li, W.; Ryabchuk, P.; Junge, K.; Beller, M. Bridging Homogeneous and Heterogeneous Catalysis by Heterogeneous Single-Metal-Site Catalysts. *Nat. Catal.* **2018**, *1* (6), 385−397.
(11) Copéret, C.; Chabanas, M.; Petroff Saint-Arroman, R.; Basset, J.-M. Homogeneous and Heterogeneous Catalysis: Bridging the Gap through Surface Organometallic Chemistry. *Angew. Chem., Int. Ed.* **2003**, *42* (2), 156−181.
(12) Chen, Z.; Vorobyeva, E.; Mitchell, S.; Fako, E.; Ortuño, M. A.; López, N.; Collins, S. M.; Midgley, P. A.; Richard, S.; Vilé, G.; Pérez-Ramírez, J. A Heterogeneous Single-Atom Palladium Catalyst Surpassing Homogeneous Systems for Suzuki Coupling. *Nat. Nanotechnol.* **2018**, *13* (8), 702−707.
(13) Basset, J.-M.; Lefebvre, F.; Santini, C. Surface Organometallic Chemistry: Some Fundamental Features Including the Coordination Effects of the Support. *Coord. Chem. Rev.* **1998**, *178*−*180*, 1703−1723.
(14) Copéret, C.; Comas-Vives, A.; Conley, M. P.; Estes, D. P.; Fedorov, A.; Mougel, V.; Nagae, H.; Núñez-Zarur, F.; Zhizhko, P. A. Surface Organometallic and Coordination Chemistry toward Single-Site Heterogeneous Catalysts: Strategies, Methods, Structures, and Activities. *Chem. Rev.* **2016**, *116* (2), 323−421.
(15) Centi, G.; Čejka, J. Needs and Gaps for Catalysis in Addressing Transitions in Chemistry and Energy from a Sustainability Perspective. *ChemSusChem* **2019**, *12* (3), 621−632.
(16) Li, X.; Rong, H.; Zhang, J.; Wang, D.; Li, Y. Modulating the Local Coordination Environment of Single-Atom Catalysts for Enhanced Catalytic Performance. *Nano Res.* **2020**, *13* (7), 1842−1855.
(17) Yang, T.; Mao, X.; Zhang, Y.; Wu, X.; Wang, L.; Chu, M.; Pao, C.-W.; Yang, S.; Xu, Y.; Huang, X. Coordination Tailoring of Cu Single Sites on C3N4 Realizes Selective CO2 Hydrogenation at Low Temperature. *Nat. Commun.* **2021**, *12* (1), 6022.
(18) Di Liberto, G.; Cipriano, L. A.; Pacchioni, G. Single Atom Catalysts: What Matters Most, the Active Site or The Surrounding? *ChemCatChem* **2022**, *14* (19), No. e202200611.
(19) Gawande, M. B.; Fornasiero, P.; Zbořil, R. Carbon-Based Single-Atom Catalysts for Advanced Applications. *ACS Catal.* **2020**, *10* (3), 2231−2259.
(20) Zhao, Z.; Sun, Y.; Dong, F. Graphitic Carbon Nitride Based Nanocomposites: A Review. *Nanoscale* **2015**, *7* (1), 15−37.
(21) Mishra, A.; Mehta, A.; Basu, S.; Shetti, N. P.; Reddy, K. R.; Aminabhavi, T. M. Graphitic Carbon Nitride (g-C3N4)-Based Metal-Free Photocatalysts for Water Splitting: A Review. *Carbon* **2019**, *149*, 693−721.
(22) Ong, W.-J.; Tan, L.-L.; Ng, Y. H.; Yong, S.-T.; Chai, S.-P. Graphitic Carbon Nitride (g-C 3 N 4)-Based Photocatalysts for Artificial Photosynthesis and Environmental Remediation: Are We a Step Closer To Achieving Sustainability? *Chem. Rev.* **2016**, *116* (12), 7159−7329.
(23) Fei, H.; Dong, J.; Chen, D.; Hu, T.; Duan, X.; Shakir, I.; Huang, Y.; Duan, X. Single Atom Electrocatalysts Supported on Graphene or Graphene-like Carbons. *Chem. Soc. Rev.* **2019**, *48* (20), 5207−5241.
(24) Hossain, M. D.; Liu, Z.; Zhuang, M.; Yan, X.; Xu, G.-L.; Gadre, C. A.; Tyagi, A.; Abidi, I. H.; Sun, C.-J.; Wong, H.; Guda, A.; Hao, Y.; Pan, X.; Amine, K.; Luo, Z. Rational Design of Graphene-Supported Single Atom Catalysts for Hydrogen Evolution Reaction. *Adv. Energy Mater.* **2019**, *9* (10), 1803689.
(25) Zhang, L.; Wang, Y.; Niu, Z.; Chen, J. Single Atoms on Graphene for Energy Storage and Conversion. *Small Methods* **2019**, *3* (9), 1800443.
(26) Ling, C.; Li, Q.; Du, A.; Wang, J. Computation-Aided Design of Single-Atom Catalysts for One-Pot CO2 Capture, Activation, and Conversion. *ACS Appl. Mater. Interfaces* **2018**, *10* (43), 36866−36872.
(27) Ling, C.; Ouyang, Y.; Li, Q.; Bai, X.; Mao, X.; Du, A.; Wang, J. A General Two-Step Strategy-Based High-Throughput Screening of Single Atom Catalysts for Nitrogen Fixation. *Small Methods* **2019**, *3* (9), 1800376.
(28) Cheng, N.; Stambula, S.; Wang, D.; Banis, M. N.; Liu, J.; Riese, A.; Xiao, B.; Li, R.; Sham, T.-K.; Liu, L.-M.; Botton, G. A.; Sun, X. Platinum Single-Atom and Cluster Catalysis of the Hydrogen Evolution Reaction. *Nat. Commun.* **2016**, *7* (1), 13638.
(29) Chen, Y.; Matanovic, I.; Weiler, E.; Atanassov, P.; Artyushkova, K. Mechanism of Oxygen Reduction Reaction on Transition Metal-Nitrogen-Carbon Catalysts: Establishing the Role of Nitrogen-Containing Active Sites. *ACS Appl. Energy Mater.* **2018**, *1* (11), 5948−5953.
(30) Rojas-Carbonell, S.; Artyushkova, K.; Serov, A.; Santoro, C.; Matanovic, I.; Atanassov, P. Effect of PH on the Activity of Platinum Group Metal-Free Catalysts in Oxygen Reduction Reaction. *ACS Catal.* **2018**, *8* (4), 3041−3053.
(31) Asset, T.; Garcia, S. T.; Herrera, S.; Andersen, N.; Chen, Y.; Peterson, E. J.; Matanovic, I.; Artyushkova, K.; Lee, J.; Minteer, S. D.; Dai, S.; Pan, X.; Chavan, K.; Calabrese Barton, S.; Atanassov, P. Investigating the Nature of the Active Sites for the CO 2 Reduction Reaction on Carbon-Based Electrocatalysts. *ACS Catal.* **2019**, *9* (9), 7668−7678.
(32) Tosoni, S.; Di Liberto, G.; Matanovic, I.; Pacchioni, G. Modelling Single Atom Catalysts for Water Splitting and Fuel Cells: A Tutorial Review. *J. Power Sources* **2023**, *556*, 232492.
(33) Greeley, J.; Jaramillo, T. F.; Bonde, J.; Chorkendorff, I.; Nørskov, J. K. Computational High-Throughput Screening of Electrocatalytic Materials for Hydrogen Evolution. *Nat. Mater.* **2006**, *5* (11), 909−913.
(34) Xu, L.; Yang, L.-M.; Ganz, E. Mn-Graphene Single-Atom Catalyst Evaluated for CO Oxidation by Computational Screening. *Theor. Chem. Acc.* **2018**, *137* (7), 98.
(35) Zafari, M.; Kumar, D.; Umer, M.; Kim, K. S. Machine Learning-Based High Throughput Screening for Nitrogen Fixation on Boron-Doped Single Atom Catalysts. *J. Mater. Chem. A* **2020**, *8* (10), 5209−5216.
(36) Niu, H.; Wang, X.; Shao, C.; Zhang, Z.; Guo, Y. Computational Screening Single-Atom Catalysts Supported on g-CN for N2 Reduction: High Activity and Selectivity. *ACS Sustain. Chem. Eng.* **2020**, *8* (36), 13749−13758.
(37) Chen, Z.; Zhao, J.; Cabrera, C. R.; Chen, Z. Computational Screening of Efficient Single-Atom Catalysts Based on Graphitic Carbon Nitride (g-C3N4) for Nitrogen Electroreduction. *Small Methods* **2019**, *3* (6), 1800368.
(38) Zhai, X.; Li, L.; Liu, X.; Li, Y.; Yang, J.; Yang, D.; Zhang, J.; Yan, H.; Ge, G. A DFT Screening of Single Transition Atoms Supported on MoS 2 as Highly Efficient Electrocatalysts for the Nitrogen Reduction Reaction. *Nanoscale* **2020**, *12* (18), 10035−10043.
(39) Zhou, Y.; Gao, G.; Kang, J.; Chu, W.; Wang, L.-W. Computational Screening of Transition-Metal Single Atom Doped C 9 N 4 Monolayers as Efficient Electrocatalysts for Water Splitting. *Nanoscale* **2019**, *11* (39), 18169−18175.
(40) Wang, Z.; Zhao, J.; Cai, Q.; Li, F. Computational Screening for High-Activity MoS 2 Monolayer-Based Catalysts for the Oxygen Reduction Reaction via Substitutional Doping with Transition Metal. *J. Mater. Chem. A* **2017**, *5* (20), 9842−9851.

https://doi.org/10.1021/acscatal.3c04801
ACS Catal. 2024, 14, 45−55

(41) Dasgupta, A.; Gao, Y.; Broderick, S. R.; Pitman, E. B.; Rajan, K. Machine Learning-Aided Identification of Single Atom Alloy Catalysts. *J. Phys. Chem. C* **2020**, *124* (26), 14158−14166.
(42) Wu, L.; Guo, T.; Li, T. Machine Learning-Accelerated Prediction of Overpotential of Oxygen Evolution Reaction of Single-Atom Catalysts. *iScience* **2021**, *24* (5), 102398.
(43) Wu, L.; Guo, T.; Li, T. Rational Design of Transition Metal Single-Atom Electrocatalysts: A Simulation-Based, Machine Learning-Accelerated Study. *J. Mater. Chem. A* **2020**, *8* (37), 19290−19299.
(44) Ying, Y.; Fan, K.; Luo, X.; Qiao, J.; Huang, H. Unravelling the Origin of Bifunctional OER/ORR Activity for Single-Atom Catalysts Supported on C 2 N by DFT and Machine Learning. *J. Mater. Chem. A* **2021**, *9* (31), 16860−16867.
(45) Di Liberto, G.; Barlocco, I.; Giordano, L.; Tosoni, S.; Pacchioni, G. Single-Atom Electrocatalysis from First Principles: Current Status and Open Challenges. *Curr. Opin. Electrochem.* **2023**, *40*, 101343.
(46) Zhuo, H.-Y.; Zhang, X.; Liang, J.-X.; Yu, Q.; Xiao, H.; Li, J. Theoretical Understandings of Graphene-Based Metal Single-Atom Catalysts: Stability and Catalytic Performance. *Chem. Rev.* **2020**, *120* (21), 12315−12341.
(47) Liu, J.-C.; Tang, Y.; Wang, Y.-G.; Zhang, T.; Li, J. Theoretical Understanding of the Stability of Single-Atom Catalysts. *Natl. Sci. Rev.* **2018**, *5* (5), 638−641.
(48) Su, Y.-Q.; Wang, Y.; Liu, J.-X.; Filot, I. A. W.; Alexopoulos, K.; Zhang, L.; Muravev, V.; Zijlstra, B.; Vlachos, D. G.; Hensen, E. J. M. Theoretical Approach To Predict the Stability of Supported Single-Atom Catalysts. *ACS Catal.* **2019**, *9* (4), 3289−3297.
(49) Liu, K.; Zhao, X.; Ren, G.; Yang, T.; Ren, Y.; Lee, A. F.; Su, Y.; Pan, X.; Zhang, J.; Chen, Z.; Yang, J.; Liu, X.; Zhou, T.; Xi, W.; Luo, J.; Zeng, C.; Matsumoto, H.; Liu, W.; Jiang, Q.; Wilson, K.; Wang, A.; Qiao, B.; Li, W.; Zhang, T. Strong Metal-Support Interaction Promoted Scalable Production of Thermally Stable Single-Atom Catalysts. *Nat. Commun.* **2020**, *11* (1), 1263.
(50) Dobrota, A. S.; Đokić, T.; Skorodumova, N. V.; Mentus, S. V.; Pašti, I. A. What Is the Real State of Single-Atom Catalysts under Electrochemical Conditions—From Adsorption to Surface Pourbaix Plots? *Catalysts* **2021**, *11* (10), 1207.
(51) Dobrota, A. S.; Skorodumova, N. V.; Mentus, S. V.; Pašti, I. A. Surface Pourbaix Plots of M@N4-Graphene Single-Atom Electrocatalysts from Density Functional Theory Thermodynamic Modeling. *Electrochim. Acta* **2022**, *412*, 140155.
(52) Holby, E. F.; Wang, G.; Zelenay, P. Acid Stability and Demetalation of PGM-Free ORR Electrocatalyst Structures from Density Functional Theory: A Model for "Single-Atom Catalyst" Dissolution. *ACS Catal.* **2020**, *10* (24), 14527−14539.
(53) Cho, J.; Lim, T.; Kim, H.; Meng, L.; Kim, J.; Lee, S.; Lee, J. H.; Jung, G. Y.; Lee, K.-S.; Viñes, F.; Illas, F.; Exner, K. S.; Joo, S. H.; Choi, C. H. Importance of Broken Geometric Symmetry of Single-Atom Pt Sites for Efficient Electrocatalysis. *Nat. Commun.* **2023**, *14* (1), 3233.
(54) DeRita, L.; Resasco, J.; Dai, S.; Boubnov, A.; Thang, H. V.; Hoffman, A. S.; Ro, I.; Graham, G. W.; Bare, S. R.; Pacchioni, G.; Pan, X.; Christopher, P. Structural Evolution of Atomically Dispersed Pt Catalysts Dictates Reactivity. *Nat. Mater.* **2019**, *18* (7), 746−751.
(55) Bae, G.; Han, S.; Oh, H.; Choi, C. H. Operando Stability of Single-Atom Electrocatalysts. *Angew. Chem.* **2023**, *135*, No. e202219227.
(56) Gana, S. J.; Egiebor, N. O.; Ankumah, R. Effect of High Temperature Treatment on Aqueous Corrosion of Low-Carbon Steel by Electrochemical Impedance Spectroscopy. *Mater. Sci. Appl.* **2011**, *02* (02), 81−86.
(57) Pourbaix, M. Applications of Electrochemistry in Corrosion Science and in Practice. *Corros. Sci.* **1974**, *14* (1), 25−82.
(58) Delahay, P.; Pourbaix, M.; Rysselberghe, P. V. Potential-pH Diagram of Lead and its Applications to the Study of Lead Corrosion and to the Lead Storage Battery. *J. Electrochem. Soc.* **1951**, *98* (2), 57.
(59) Persson, K. A.; Waldwick, B.; Lazic, P.; Ceder, G. Prediction of Solid-Aqueous Equilibria: Scheme to Combine First-Principles Calculations of Solids with Experimental Aqueous States. *Phys. Rev. B* **2012**, *85* (23), 235438.
(60) Kresse, G.; Hafner, J. Ab Initio Molecular Dynamics for Liquid Metals. *Phys. Rev. B* **1993**, *47* (1), 558−561.
(61) Kresse, G.; Hafner, J. Ab Initio Molecular-Dynamics Simulation of the Liquid-Metal-Amorphous-Semiconductor Transition in Germanium. *Phys. Rev. B* **1994**, *49* (20), 14251−14269.
(62) Kresse, G.; Furthmüller, J. Efficiency of Ab-Initio Total Energy Calculations for Metals and Semiconductors Using a Plane-Wave Basis Set. *Comput. Mater. Sci.* **1996**, *6* (1), 15−50.
(63) Perdew, J. P.; Burke, K.; Ernzerhof, M. Generalized Gradient Approximation Made Simple. *Phys. Rev. Lett.* **1996**, *77* (18), 3865−3868.
(64) Grimme, S.; Antony, J.; Ehrlich, S.; Krieg, H. A Consistent and Accurate Ab Initio Parametrization of Density Functional Dispersion Correction (DFT-D) for the 94 Elements H-Pu. *J. Chem. Phys.* **2010**, *132* (15), 154104.
(65) Blöchl, P. E. Projector Augmented-Wave Method. *Phys. Rev. B* **1994**, *50* (24), 17953−17979.
(66) Kresse, G.; Joubert, D. From Ultrasoft Pseudopotentials to the Projector Augmented-Wave Method. *Phys. Rev. B* **1999**, *59* (3), 1758−1775.
(67) Monkhorst, H. J.; Pack, J. D. Special Points for Brillouin-Zone Integrations. *Phys. Rev. B* **1976**, *13* (12), 5188−5192.
(68) Van Dao, D.; Cipriano, L. A.; Di Liberto, G.; Nguyen, T. T. D.; Ki, S.-W.; Son, H.; Kim, G.-C.; Lee, K. H.; Yang, J.-K.; Yu, Y.-T.; Pacchioni, G.; Lee, I.-H. Plasmonic Au Nanoclusters Dispersed in Nitrogen-Doped Graphene as a Robust Photocatalyst for Light-to-Hydrogen Conversion. *J. Mater. Chem. A* **2021**, *9* (40), 22810−22819.
(69) Van Dao, D.; Di Liberto, G.; Ko, H.; Park, J.; Wang, W.; Shin, D.; Son, H.; Van Le, Q.; Van Nguyen, T.; Van Tan, V.; Pacchioni, G.; Lee, I.-H. LaFeO 3 Meets Nitrogen-Doped Graphene Functionalized with Ultralow Pt Loading in an Impactful Z-Scheme Platform for Photocatalytic Hydrogen Evolution. *J. Mater. Chem. A* **2022**, *10* (7), 3330−3340.
(70) Barlocco, I.; Cipriano, L. A.; Di Liberto, G.; Pacchioni, G. Does the Oxygen Evolution Reaction Follow the Classical OH*, O*, OOH* Path on Single Atom Catalysts? *J. Catal.* **2023**, *417*, 351−359.
(71) Di Liberto, G.; Tosoni, S.; Pacchioni, G. Z-Scheme versus Type-II Junction in g-C 3 N 4/TiO 2 and g-C 3 N 4/SrTiO 3/TiO 2 Heterostructures. *Catal. Sci. Technol.* **2021**, *11* (10), 3589−3598.
(72) Vilé, G.; Di Liberto, G.; Tosoni, S.; Sivo, A.; Ruta, V.; Nachtegaal, M.; Clark, A. H.; Agnoli, S.; Zou, Y.; Savateev, A.; Antonietti, M.; Pacchioni, G. Azide-Alkyne Click Chemistry over a Heterogeneous Copper-Based Single-Atom Catalyst. *ACS Catal.* **2022**, *12* (5), 2947−2958.
(73) Wang, J.; Zhang, Z.; Li, Y.; Qu, Y.; Li, Y.; Li, W.; Zhao, M. Screening of Transition-Metal Single-Atom Catalysts Anchored on Covalent-Organic Frameworks for Efficient Nitrogen Fixation. *ACS Appl. Mater. Interfaces* **2022**, *14* (1), 1024−1033.
(74) Lu, M.; Zhang, M.; Liu, C.; Liu, J.; Shang, L.; Wang, M.; Chang, J.; Li, S.; Lan, Y. Stable Dioxin-Linked Metallophthalocyanine Covalent Organic Frameworks (COFs) as Photo-Coupled Electrocatalysts for CO $_2$ Reduction. *Angew. Chem.* **2021**, *133* (9), 4914−4921.
(75) Barlocco, I.; Di Liberto, G.; Pacchioni, G. Hydrogen and Oxygen Evolution Reactions on Single Atom Catalysts Stabilized by a Covalent Organic Framework. *Energy Adv.* **2023**, *2*, 1022−1029.
(76) Di Liberto, G.; Cipriano, L. A.; Pacchioni, G. Role of Dihydride and Dihydrogen Complexes in Hydrogen Evolution Reaction on Single-Atom Catalysts. *J. Am. Chem. Soc.* **2021**, *143* (48), 20431−20441.
(77) Cipriano, L. A.; Di Liberto, G.; Pacchioni, G. Superoxo and Peroxo Complexes on Single Atom Catalysts: Impact on the Oxygen Evolution Reaction. *ACS Catal.* **2022**, *12*, 11682−11691.
(78) Nørskov, J. K.; Bligaard, T.; Rossmeisl, J.; Christensen, C. H. Towards the Computational Design of Solid Catalysts. *Nat. Chem.* **2009**, *1* (1), 37−46.

(79) Nørskov, J. K.; Rossmeisl, J.; Logadottir, A.; Lindqvist, L.; Kitchin, J. R.; Bligaard, T.; Jónsson, H. Origin of the Overpotential for Oxygen Reduction at a Fuel-Cell Cathode. *J. Phys. Chem. B* **2004**, *108* (46), 17886−17892.
(80) Lejaeghere, K.; Van Speybroeck, V.; Van Oost, G.; Cottenier, S. Error Estimates for Solid-State Density-Functional Theory Predictions: An Overview by Means of the Ground-State Elemental Crystals. *Crit. Rev. Solid State Mater. Sci.* **2014**, *39* (1), 1−24.
(81) Janthon, P.; Luo, S. (A.).; Kozlov, S. M.; Viñes, F.; Limtrakul, J.; Truhlar, D. G.; Illas, F. Bulk Properties of Transition Metals: A Challenge for the Design of Universal Density Functionals. *J. Chem. Theory Comput.* **2014**, *10* (9), 3832−3839.
(82) Hasija, V.; Patial, S.; Raizada, P.; Aslam Parwaz Khan, A.; Asiri, A. M.; Van Le, Q.; Nguyen, V.-H.; Singh, P. Covalent Organic Frameworks Promoted Single Metal Atom Catalysis: Strategies and Applications. *Coord. Chem. Rev.* **2022**, *452*, 214298.
(83) Lin, C.; Zhang, L.; Zhao, Z.; Xia, Z. Design Principles for Covalent Organic Frameworks as Efficient Electrocatalysts in Clean Energy Conversion and Green Oxidizer Production. *Adv. Mater.* **2017**, *29* (17), 1606635.
(84) Govindarajan, N.; García-Lastra, J. M.; Meijer, E. J.; Calle-Vallejo, F. Does the Breaking of Adsorption-Energy Scaling Relations Guarantee Enhanced Electrocatalysis? *Curr. Opin. Electrochem.* **2018**, *8*, 110−117.
(85) Exner, K. S. A Universal Descriptor for the Screening of Electrode Materials for Multiple-Electron Processes: Beyond the Thermodynamic Overpotential. *ACS Catal.* **2020**, *10* (21), 12607−12617.
(86) Su, Y.-Q.; Zhang, L.; Wang, Y.; Liu, J.-X.; Muravev, V.; Alexopoulos, K.; Filot, I. A. W.; Vlachos, D. G.; Hensen, E. J. M. Stability of Heterogeneous Single-Atom Catalysts: A Scaling Law Mapping Thermodynamics to Kinetics. *npj Comput. Mater.* **2020**, *6* (1), 144.
(87) Patel, A. M.; Ringe, S.; Siahrostami, S.; Bajdich, M.; Nørskov, J. K.; Kulkarni, A. R. Theoretical Approaches to Describing the Oxygen Reduction Reaction Activity of Single-Atom Catalysts. *J. Phys. Chem. C* **2018**, *122* (51), 29307−29318.
(88) Barlocco, I.; Cipriano, L. A.; Di Liberto, G.; Pacchioni, G. Modeling Hydrogen and Oxygen Evolution Reactions on Single Atom Catalysts with Density Functional Theory: Role of the Functional. *Adv. Theory Simul.* **2023**, *6*, 2200513.
(89) Gauthier, J. A.; Dickens, C. F.; Chen, L. D.; Doyle, A. D.; Nørskov, J. K. Solvation Effects for Oxygen Evolution Reaction Catalysis on IrO 2 (110). *J. Phys. Chem. C* **2017**, *121* (21), 11455−11463.
(90) Zhang, Q.; Asthagiri, A. Solvation Effects on DFT Predictions of ORR Activity on Metal Surfaces. *Catal. Today* **2019**, *323*, 35−43.
(91) Di Liberto, G.; Pacchioni, G.; Shao-Horn, Y.; Giordano, L. Role of Water Solvation on the Key Intermediates Catalyzing Oxygen Evolution on RuO_2. *J. Phys. Chem. C* **2023**, *127* (21), 10127−10133.
(92) Adamo, C.; Barone, V. Toward Reliable Density Functional Methods without Adjustable Parameters: The PBE0Model. *J. Chem. Phys.* **1999**, *110* (13), 6158−6170.
(93) Perdew, J. P.; Ernzerhof, M.; Burke, K. Rationale for Mixing Exact Exchange with Density Functional Approximations. *J. Chem. Phys.* **1996**, *105* (22), 9982−9985.
(94) Calle-Vallejo, F.; F. de Morais, R.; Illas, F.; Loffreda, D.; Sautet, P. Affordable Estimation of Solvation Contributions to the Adsorption Energies of Oxygenates on Metal Nanoparticles. *J. Phys. Chem. C* **2019**, *123* (9), 5578−5582.
(95) Di Liberto, G.; Giordano, L. Role of Solvation Model on the Stability of Oxygenates on Pt(111): A Comparison between Microsolvation, Extended Bilayer, and Extended Metal/Water Interface. *Electrochem. Sci. Adv.* **2023**, No. e2100204.
(96) Misra, D.; Di Liberto, G.; Pacchioni, G. CO2 Electroreduction on Single Atom Catalysts: Is Water Just a Solvent? *J. Catal.* **2023**, *422*, 1−11.

https://doi.org/10.1021/acscatal.3c04801
ACS Catal. 2024, 14, 45−55